

1 Comparing observed and modelled components of the Atlantic Meridional Overturning  
2 Circulation at 26°N.

3  
4 Harry Bryden<sup>1</sup>, Jordi Beunk<sup>2</sup>, Sybren Drijfhout<sup>1,2</sup>, Wilco Hazeleger<sup>2</sup>, Jennifer Mecking<sup>3</sup>

5  
6 <sup>1</sup>Ocean and Earth Science, University of Southampton, Southampton United Kingdom

7 <sup>2</sup>Faculty of Geosciences, University of Utrecht, Utrecht, The Netherlands

8 <sup>3</sup>National Oceanography Centre, Southampton, United Kingdom

9  
10 Correspondence Email: [hlb@soton.ac.uk](mailto:hlb@soton.ac.uk)

11  
12 2 February 2024

### 13 14 **Abstract**

15  
16 The Coupled Model Intercomparison Project (CMIP) allows assessment of the representation  
17 of the Atlantic Meridional Overturning Circulation (AMOC) in climate models. While CMIP  
18 Phase 6 models display a large spread in AMOC strength by a factor of three, the multi-model  
19 mean strength agrees reasonably well with observed estimates from RAPID<sup>1</sup>, but this does not  
20 hold for its various components. In CMIP6 the present-day AMOC is characterised by a lack  
21 of lower North Atlantic Deep Water (LNADW), due to the small-scale of Greenland-Iceland-  
22 Scotland Ridge overflow and too much mixing. This is compensated by increased  
23 recirculation in the subtropical gyre and more Antarctic Bottom Water (AABW). Deep-water  
24 circulation is dominated by a distinct deep western boundary current (DWBC) with minor  
25 interior recirculation compared to observations. The future decline in the AMOC to 2100 of  
26 7Sv under a SSP5-8.5 scenario is associated with decreased northward western boundary  
27 current transport in combination with reduced southward flow of upper North Atlantic Deep  
28 Water (uNADW). In CMIP6, wind stress curl decreases with time by 14% so that the wind-  
29 driven thermocline recirculation in the subtropical gyre is reduced by 4 Sv (17%) by 2100.  
30 The reduction in western boundary current transport of 11Sv is more than the decrease in the  
31 wind-driven gyre transport indicating a decrease over time in the component of the Gulf  
32 Stream originating in the South Atlantic.

### 33 34 **1. Introduction**

35  
36 The Atlantic Meridional Overturning Circulation (AMOC) is the Atlantic part of the global  
37 overturning circulation. The global overturning circulation, in which deep waters formed at  
38 high latitudes in the northern Atlantic and Weddell Sea flow equatorward, upwell, circulate  
39 and eventually flow as upper waters back toward the formation regions, transports heat,  
40 freshwater, nutrients and CO<sub>2</sub> throughout the global ocean. The AMOC includes North  
41 Atlantic Deep Water (NADW) formation in the subpolar and polar regions of the northern  
42 Atlantic, southward flow of NADW in deep western boundary currents, wind-driven  
43 circulation in the subtropical and subpolar gyres and northward flow of upper waters notably  
44 in the Gulf Stream. Upwelling of NADW occurs principally outside of the North Atlantic.  
45 Our understanding of the strength, variability and structure of the AMOC has improved since  
46 the deployment of the RAPID<sup>1</sup> array, which monitors the volume transport at 26°N since

---

<sup>1</sup> RAPID is used here as shorthand for the RAPID-Meridional Overturning Circulation and Heatflux Array-Western Boundary Time Series at 26°N (Moat et al., 2022).

47 April 2004 (Moat et al., 2020). Additionally, these observations serve as invaluable reference  
48 data for the representation of the AMOC in coupled climate and Earth System models. The  
49 most recent phase of the Coupled Model Intercomparison Project, CMIP Phase 6, allows us to  
50 assess the representation of the AMOC in these models. The models project the AMOC  
51 strength will decline over the next century (Lee et al., 2021). Here we compare observed and  
52 modeled components of the AMOC over the historical period 2004 to 2014 and then assess  
53 how the ensemble-mean CMIP6 transport components change in a declining AMOC over the  
54 next century under SSP5-8.5 emission scenario.

55

56 The RAPID AMOC observations from 2004 to 2018 indicate that the AMOC has declined by  
57 2.4 Sv, about 12%, from 18.3 Sv to 15.9 Sv (Bryden, 2021). The decline is primarily evident  
58 in reduced southward transport of lower North Atlantic Deep Water (INADW) that is  
59 balanced by slightly reduced Gulf Stream transport and more southward recirculation within  
60 the subtropical gyre. In CMIP6 models, the AMOC declines by about 40% over the 21st  
61 century (Weijer et al., 2020). Here we analyse 19 CMIP6 model projections in order to  
62 identify which components lead to the AMOC decline, for clues as to how the AMOC may  
63 change within the continuing RAPID observational framework.

64

65 The Coupled Model Intercomparison Project (CMIP) is a comprehensive effort of modelling  
66 centres around the world to improve our understanding about past, present and future changes  
67 of the climate system (Eyring et al., 2016; O'Neill et al., 2016). Even though CMIP6 shows  
68 improvements compared to previous CMIP generations, model biases related to the AMOC  
69 persist. These include a shallow bias to the deep cell, too much deep convection, and a too-  
70 small temperature difference between its upper and lower limbs. Additionally, CMIP6  
71 models largely underestimate low-frequency variability of the AMOC and show large inter-  
72 model differences in their AMOC representation (Weijer et al., 2020).

73

74 The RAPID array monitors the AMOC volume transport at 26°N since April 2004 (Smeed et  
75 al., 2018). The transport through the cross section is estimated by a decomposition of the  
76 AMOC into 3 components: (1) transport through the Florida Straits, (2) Ekman surface  
77 transport generated by zonal wind stress, and (3) density driven interior transport estimated  
78 from mooring measurements. The mid-ocean interior transport is further broken down into  
79 thermocline recirculation (0-800m depth), intermediate water transport (800-1100m), upper  
80 North Atlantic Deep Water (1100-3000m), lower North Atlantic Deep Water (3000-5000m).  
81 The goal of this study is to gain insight into the cause of disagreement between CMIP6  
82 models and RAPID data in terms of AMOC strength, structure and variability. We  
83 decompose the modelled AMOC transport at 26°N from CMIP6 into the same transport  
84 components as measured by the RAPID array. We compare the CMIP6 transport components  
85 with the observed RAPID components for the historical period 2004-2014. We then examine  
86 the change of these components in CMIP6 under the SSP5-8.5 emission scenario from the  
87 historical period until 2100.

88

## 89 **2. Data and Methods**

90

91 Monthly averages of AMOC estimates from the RAPID array are compared to the historical  
92 simulations of 19 CMIP6 models. Note that only the overlapping period was investigated,  
93 April 2004 – December 2014. Details of the 19 CMIP6 models are given in Table 1. The  
94 SSP5-8.5 future projection from 2015 to 2100, is then used to investigate how the AMOC  
95 may change in future projections. For each model, one ensemble member was used as  
96 defined in Table 1.

<i>Model</i>	<i>Modelling centre</i>	<i>Horizontal resolution (°)</i>	<i>Variant label</i>	<i>Data reference historical</i>	<i>Data reference SSP585</i>
CAMS-CSM1-0	CAMS	1 x 1	r1i1p1f1	Rong (2019)	Rong (2019)
CAS-ESM2-0	CAS	1 x 1	r1i1p1f1	Chai (2020)	Unknown (2018)
CESM2-WACCM	NCAR	1 x 1	r1i1p1f1	Danabasoglu (2019)	Danabasoglu (2019)
CIESM	THU	1 x 1	r1i1p1f1	Huang (2019)	Huang (2020)
CMCC-CM2-SR5	CMCC	1 x 1	r1i1p1f1	Lovato and Peano (2020)	Lovato and Peano (2020)
CMCC-ESM2	CMCC	1 x 1	r1i1p1f1	Lovato et al. (2021)	Lovato et al. (2021)
CNRM-CM6-1	CNRM-CERFACS	1 x 1	r1i1p1f2	Voltaire (2019)	Voltaire (2019)
CNRM-ESM2-1	CNRM-CERFACS	1 x 1	r2i1p1f2	Seferian (2018)	-
CanESM5	CCCma	1 x 1	r1i1p1f1	Swart et al. (2019)	Swart et al. (2019)
EC-Earth3	EC-Earth Consortium	1 x 1	r1i1p1f1	EC-Earth Consortium (2021)	EC-Earth Consortium (2019)
FIO-ESM-2-0	FIO-QINM	1 x 1	r1i1p1f1	Song et al. (2019)	Song et al. (2019)
HadGEM3-GC31-LL	MOHC	1 x 1	r1i1p1f3	Ridley et al. (2019)	Good (2020)
HadGEM3-GC31-MM	MOHC	0.25 x 0.25	r1i1p1f3	Ridley et al. (2019)	Ridley et al. (2019)
IPSL-CM6A-LR	IPSL	1 x 1	r1i1p1f1	Boucher et al. (2021)	Boucher et al. (2019)
MPI-ESM1-2-HR	MPI	0.4 x 0.4	r1i1p1f1	Jungclaus et al. (2019)	Schupfner et al. (2019)
MPI-ESM1-2-LR	MPI	1.5 x 1.5	r1i1p1f1	Wieners et al. (2019)	Wieners et al. (2019)
MRI-ESM2-0	MRI	1 x 0.5	r1i1p1f1	Yukimoto et al. (2019)	Yukimoto et al. (2019)
NESM3	NUIST	1 x 1	r1i1p1f1	Cao and Wang (2019)	Cao (2019)
UKESM1-0-LL	MOHC	1 x 1	r1i1p1f2	Tang et al. (2019)	Good et al. (2019)

97

98

99

100

101

102

103

104

105

106

107

108

109

110

111

112

113

114

115

116

117

118

119

120

121

122

123

124

125

126

127

128

129

Table 1. Metadata and references for the models analysed in this study. The choice of models is motivated by the fact that historical and SSP85 data is available for all used variables including meridional velocity, zonal wind stress, salinity and temperature. In addition only models that use horizontal depth values are included. The choice of ensemble member is indicated and the preferred ensemble member is realisation 1, initialisation 1, physics 1 and forcing 1, indicated by r1i1p1f1. For some models forcing 1 was not available so a different ensemble member was chosen making sure that the forcing version (v6.2.0) is the same. References are from the Earth System Grid Federation.

A cross section between Florida and the African continent at the latitude closest to 26°N was selected for each model. The net transport through the section, approximately -1 Sv for each model due to the Bering Strait throughflow, was removed before computing the AMOC components from meridional velocities as follows:

Florida Straits Transport (FS): CMIP6 models do not resolve the Bahama Islands and as a result the Florida Straits proper. For this reason the following definition is used. The boundary between Florida Straits (FS) transport and mid-ocean transport is defined as the longitude where the depth-averaged transport (from the surface down to the depth of maximum overturning) changes from positive (northward) to negative (southward). This definition thus identifies the FS transport as the western boundary current, thereby including the transport by the Antilles Current, which in CMIP6 models cannot be separated from the Florida Current.

For each model, we have made the following choices to define Thermocline Recirculation, Upper North Atlantic Deep Water, Lower North Atlantic Deep Water and Antarctic Bottom Water. The decision was to use potential temperature to determine the boundaries between upper and lower North Atlantic Deep Water in the CMIP6 models. This choice was motivated by the indistinct upper boundary (in depth) of Lower North Atlantic Deep Water in the models.

Thermocline Recirculation (tr): East of FS and from the surface to down to the depth of horizontally averaged potential temperature of 8°C.

130  
131 Intermediate Waters (iw): East of FS and between the depth of horizontally averaged potential  
132 temperature of 8°C and depth of maximum overturning.

133  
134 Upper North Atlantic Deep Water (uNADW): Between the depth of maximum overturning  
135 and the depth of horizontally averaged potential temperature of 3°C.

136  
137 Lower North Atlantic Deep Water (lNADW): Between the depth of horizontally averaged  
138 potential temperature of 3°C and the depth where horizontally-averaged transport changes  
139 from negative to positive.

140  
141 Antarctic Bottom Water (AABW): Between the depth where horizontally-averaged transport  
142 changes from negative to positive and the bottom.

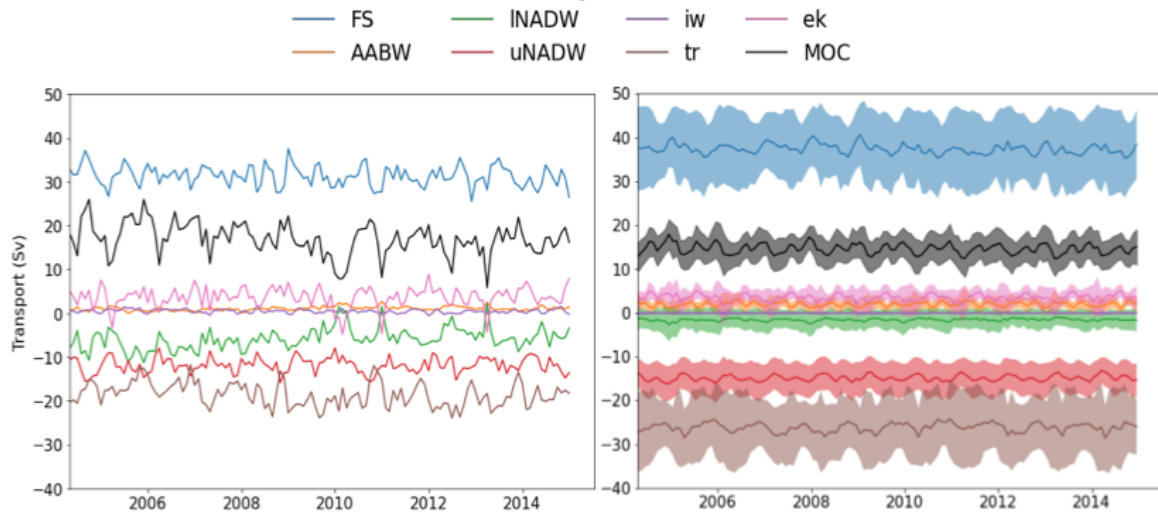
143  
144 Ekman (ek): Near surface ageostrophic transport estimated from the zonal wind stress.

145  
146 Multi-model means (MMM) for each component over the 19 models are then made with their  
147 standard deviation.

### 148 149 **3. Results**

150  
151 Figure 1 compares the RAPID observations of the AMOC transport components with the  
152 CMIP6 components for the historical period 2004-2014. For the historical period (2004-  
153 2014) the MMM CMIP6 AMOC underestimates the observed AMOC transport by 2.2 Sv  
154 (Table 2). The underestimation of AMOC strength in the CMIP6 models is likely related to  
155 the reduced transport of lower NADW, due to the small scale of Greenland-Iceland-Scotland  
156 Ridge overflow compared to the resolution of models and excessive mixing at this location. In  
157 a study of deep waters in CMIP6, Heuzé (2021) noted that the models did form water masses  
158 similar in properties to lNADW in the Nordic Seas, but none of the deep waters made it over  
159 the ridge and into the Iceland or Irminger basins. In the models, this lack of lNADW is  
160 partially compensated by increased southward flow of upper NADW so the total southward  
161 flow of deep water in CMIP6 is comparable to that observed by RAPID. The variability of  
162 NADW is underestimated, most likely due to the inability of models to reproduce lower  
163 NADW overflow. Deep-water circulation in models is dominated by a distinct DWBC with  
164 minor interior recirculation compared with observations. CMIP6 MMM Florida Straits (FS)  
165 transport (37.4 Sv) is larger than observed Florida Straits transport (31.3 Sv). The relatively  
166 coarse-resolution models do not resolve the narrow Florida Straits, and the model western  
167 boundary current includes the narrow Antilles Current east of the Bahamas as well as the Gulf  
168 Stream flow through Florida Straits. The Antilles Current has maximum northward velocity at  
169 360m depth and the core of the Current is within 50 km of the Bahama Islands. Recent  
170 estimates of Antilles Current transport are about 5 Sv (Meinen et al., 2019) and adding this  
171 transport to the observed Florida Straits transport suggests that the observed (36.3 Sv) and  
172 modeled (37.4 Sv) western boundary current transports are similar. The low-frequency  
173 variability of Florida Straits transport is largely overestimated in CMIP6 models and we  
174 hypothesize that the inclusion of the Antilles Current in this component in models may be a  
175 significant contributor to this variability as the observed Antilles Current transport exhibits  
176 rms variability of 7.5 Sv that is not correlated with Florida Straits transport variability. The  
177 MMM thermocline recirculation (tr) in CMIP6 models (-26.2 Sv) is larger than observed by  
178 the RAPID array (-18.6 Sv) though again this may be due to issues on how the Antilles  
179 Current transport is accounted in the observations and in the models. RAPID estimates

180 thermocline recirculation to be the overall southward flow above 800m depth between the  
 181 Bahamas and Africa and this overall flow includes both the Antilles Current transport and the  
 182 mid-ocean thermocline recirculation associated with the wind-driven subtropical gyre. If we  
 183 separate out the northward Antilles Current transport of 5 Sv, then the mid-ocean thermocline  
 184 recirculation for RAPID would be -23.6 Sv (Table 2) in more reasonable agreement with the  
 185 CMIP6 MMM thermocline circulation of -26.2 Sv. Overall, the MMM circulation in CMIP6  
 186 models for the historical period reasonably represents the observed circulation in RAPID  
 187 except for the underestimated INADW transport associated with issues of model  
 188 representation of flows over ridges.  
 189



190  
 191 Figure 1. Historical time series for RAPID data (left) and multi-model mean CMIP6 data  
 192 (right). Shaded areas indicate one standard deviation of the ensemble spread.

	Rapid (2004-14)	CMIP6 Average		
		Historical (2004-14)	2090-2100	Decline
Upper Water				
Florida Straits (FS)	31.3			
Ekman	3.6	3.5	3.4	0.1 (1%)
Intermediate Water (IW)	0.4	----	----	
Thermocline Recirculation (TR)	-18.6			
AMOC=FS+Ekman+IW+TR	16.7			
Antilles Current (AC)	5			
Western Boundary Current (FS+AC)	36.3	37.4	26.4	11 (30%)
Thermocline Recirculation +AC	-23.6			
Model Thermocline Recirculation		-26.2	-21.8	4.4 (17%)
Western Boundary Current+Ekman+Model TR		14.7	8.0	6.7 (45%)
Deep Water				
uNADW	-11.9	-14.9	-9.9	5.0 (34%)
INADW	-5.9	-1.6	-0.2	1.4 (85%)
AABW	1.0	1.9	2.1	-0.2 (9%)
AMOC=uNADW+INADW+AABW	-16.8	-14.6	-8.0	6.6 (45%)

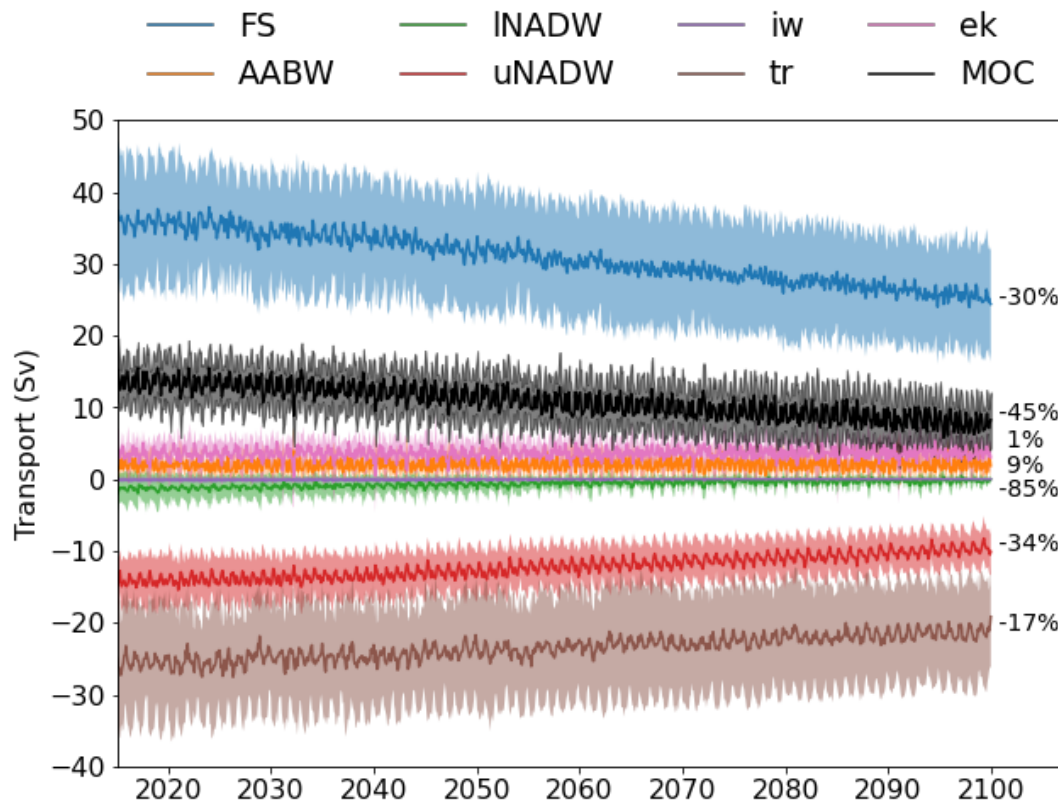
193  
 194 Table 2. Components of the Atlantic Meridional Overturning Circulation at 26°N. Model  
 195 western boundary current includes both Florida Straits and Antilles Current transports. The  
 196 observed Antilles Current (AC) transport of 5 Sv is a rounded value from Meinen et al.  
 197 (2019)'s mean transport of  $4.7 \pm 7.5$  Sv. For standard RAPID analyses, thermocline  
 198 recirculation includes Antilles Current transport.

199  
200  
201  
202  
203  
204  
205  
206  
207

CMIP6 model projections suggest that the AMOC will decline over the next century as noted by Weijer et al. (2020). Here we find that the AMOC declines by 45% over the period 2015 to 2100 in a MMM of 19 CMIP6 projections. For comparison, over the RAPID time period 2004 to 2021, the AMOC has exhibited a small (order 12%) reduction that is manifest principally in reduced southward transport of INADW (Bryden, 2021). It is of interest to identify which components contribute to the projected 45% decline in the AMOC over the coming century in CMIP6 simulations.

208  
209  
210  
211  
212  
213  
214  
215  
216  
217  
218  
219  
220  
221

All 19 CMIP6 models analysed here exhibit a decline in the AMOC over the 21st century (Table 3). This decline of the AMOC under SSP5-8.5 is in line with other modelling studies (Levang and Schmitt, 2020; Weijer et al, 2020; Roberts et al., 2020). Averaged over the 19 models, the AMOC decline from 2004-2014 to 2090-2100 is 6.6 Sv or 45% in the AMOC transport for the historical period (Figure 2). We find that the decline in the AMOC at 26°N in CMIP6 models from 2015 to 2100 is dominated by a 30% decrease in western boundary current transport (FS in Figure 2) and a 34% reduction in southward deep water transport (uNADW in Figure 2). As Ekman transport (ek) shows no significant change in the model projections, the AMOC decline of 6.6 Sv in the upper waters is the result of the difference between the decline in western boundary current (FS) transport of 11.0 Sv and the 17% decline in southward thermocline recirculation (tr) of 4.4 Sv. For the lower waters the overall decline in northward transport of upper waters of 6.6 Sv is compensated by a decrease in uNADW transport of 6.4 Sv and a small increase in northward AABW transport of 0.2 Sv, so that the net transport through the cross section remains zero.



222  
223  
224  
225

Figure 2. Multi-model mean timeseries of each component under SSP5-8.5. Shaded areas illustrate one standard deviation of the inter-model spread. Percentages show the decline relative to the historical period.

<i>Model name</i>	<i>Historical mean (Sv)</i>	<i>2090-2100 mean (Sv)</i>	<i>Change (Sv)</i>	<i>Change (%)</i>
<i>CAMS-CSM1-0</i>	12.4	8.9	-3.5	-28
<i>CAS-ESM2-0</i>	18.4	13.7	-4.7	-26
<i>CESM2-WACCM</i>	17.9	6.8	-11.1	-62
<i>CIesm</i>	11.4	4	-7.4	-65
<i>CMCC-CM2-SR5</i>	14.2	9.2	-5.0	-35
<i>CMCC-ESM2</i>	13.3	9.3	-4.0	-30
<i>CNRM-CM6-1</i>	15.7	6.9	-8.8	-56
<i>CNRM-ESM2-1</i>	15.3			
<i>CanESM5</i>	11.4	5.5	-5.9	-52
<i>EC-Earth3</i>	16.2	10.7	-5.5	-34
<i>FIO-ESM-2-0</i>	17.7	10.7	-7.0	-39
<i>HadGEM3-GC31-LL</i>	15.2	7.9	-7.3	-48
<i>HadGEM3-GC31-MM</i>	15.4	6.5	-8.9	-58
<i>IPSL-CM6A-LR</i>	11.6	6.5	-5.1	-44
<i>MPI-ESM1-2-HR</i>	14.8	8.6	-6.2	-42
<i>MPI-ESM1-2-LR</i>	16.6	11.4	-5.2	-31
<i>MRI-ESM2-0</i>	15.4	5	-10.4	-67
<i>NESM3</i>	9.0	5	-4.0	-45
<i>UKESM1-0-LL</i>	15.6	7.8	-7.8	-50

227

228

229

230

231

Table 3. Values of the total AMOC for every model. Shown are the historical mean values, 2090-2100 mean values, absolute change and relative change. Changes are relative to the historical period.

232

233

234

235

236

237

238

239

240

241

242

243

244

245

246

247

248

To examine changes in wind-driven circulation over the 21<sup>st</sup> century in the subtropical North Atlantic, we examined the mean wind-stress curl along the 26°N section for the historical and SSP5-8.5 period. The values are negative (i.e. clockwise rotation), which results in southward mid-ocean Sverdrup transport. Since the upper level gyre circulation is driven by wind-stress curl (DiNezio et al., 2009; Zhao and Johns, 2014), we expect a decrease of this driver to affect both Florida Straits transport and thermocline recirculation. Averaged over the model projections, wind stress curl decreases by 14% from about  $6 \times 10^{-8} \text{ m s}^{-2}$ . On the basis of Sverdrup dynamics, we expect this change in wind stress curl will reduce the thermocline recirculation at 26°N and indeed the thermocline recirculation does decrease by 4.4 Sv or 17% over the 21<sup>st</sup> century. We conclude that the reduction of thermocline recirculation is almost entirely caused by a decline in wind-stress curl and the decline in the directly wind-driven component of the AMOC is exactly reflected in the 17% decline of the Thermocline Recirculation (tr in Figure 2). On the basis of western intensification theory (Stommel, 1948), the decrease in wind-stress curl should also lead to a decrease in western boundary current transport by a similar amount. Thus we can explain a decrease in western boundary current transport of 4.4 Sv over the 21<sup>st</sup> century as being due to changes in the wind forcing.

249

250

251

252

253

254

255

256

257

258

The change in the western boundary current transport of 11 Sv in the CMIP projections is due to a reduction in the wind-driven component by 4.4 Sv and to a reduction in the component of the Gulf Stream flow originating from the South Atlantic of 6.6 Sv. The overall 6.6 Sv reduction in the northward flow in the upper waters is then compensated by a reduction in southward flow of the deep waters. In CMIP6, the reduction in the southward flow of deep water is almost entirely due to a decreased DWBC transport of uNADW over the period 2015-2100. Hence the decline in the thermohaline component is reflected in the 34% decline in uNADW transport (uNADW in Figure 2). Overall, the projected AMOC reduction over the 21<sup>st</sup> century in CMIP6 is due to a reduction in the thermohaline circulation where there is less northward transport of upper waters principally in the western boundary current across 26°N

259 and less southward deep water transport in the deep western boundary current.

260

261

#### 262 **4. Discussion**

263

264 There is much interest in whether the AMOC will decline over the 21st century. Recent  
265 analyses of historical observations using Bayesian methods have concluded that the Gulf  
266 Stream has weakened by about 1 Sv over the past 40 years (Piecuch and Beal, 2023) and that  
267 the AMOC will decline markedly over the next 50 years (Ditlevsen and Ditlevsen, 2023).

268 These studies have generated great media interest. Here we use CMIP6 forward model  
269 projections under expected climate forcing (SSP5-8.5) to assess what state-of-the-art coupled  
270 climate models 'predict' for the AMOC over the 21st century. McCarthy and Caesar (2023)  
271 have argued that models like CMIP6 have not been able to simulate large AMOC variations  
272 in the paleo record and hence should not be relied upon to generate accurate projections of  
273 future AMOC. Comparisons between model projections and observed circulation variability  
274 like those presented above do provide an assessment of the models ability to reliably project  
275 the future course of the AMOC. CMIP6 models project declines in both wind-driven and  
276 thermohaline components of the AMOC out to 2100. Comparing these projections with  
277 ongoing observations like RAPID then provides a reality check on the ability of present  
278 models to define future climate change.

279

280 Over the SSP5-8.5 period (2015-2100) in CMIP6 projections, we find declines in the western  
281 boundary current transport, thermocline recirculation and NADW transport. Decreased  
282 thermocline recirculation is related to a decline in wind stress curl along the section and this  
283 decline is also expected to contribute to the decline in Gulf Stream transport. But the decline  
284 in western boundary current transport in CMIP6 models is substantially greater than the  
285 decline in wind stress curl and accompanying thermocline recirculation. Therefore, for the  
286 upper water circulation the CMIP6 decline in the AMOC is mostly caused by a decrease in  
287 the component of the western boundary current associated with the thermohaline circulation.  
288 For the lower water circulation, the decline in southward transport over the SSP5-8.5 period is  
289 associated with reduced uNADW transport. The overall reduction in southward deep water  
290 transport suggests a decline in NADW formation.

291

292 In a similar study, Asbjornsen and Arthun (2023) examined future changes in the AMOC  
293 using 14 CMIP6 models and found a weakening AMOC by 8.5 Sv over the coming century.  
294 For their ensemble, the Gulf Stream weakened by 33% or 11.2 Sv, 3.7 Sv of which was due to  
295 change in wind stress, and the Deep Western Boundary Current transport weakened by 8.5  
296 Sv. As noted above, the CMIP6 projections are consistent in projecting a decline in the  
297 AMOC this century (Table 3), but the exact size of the AMOC reduction depends on which  
298 models are used for the study.

299

300 Because the AMOC is responsible for most of the northward heat transport in the Atlantic  
301 Ocean (Johns et al., 2011; Johns et al., 2023), CMIP6 model projections also exhibit a  
302 decrease in northward heat transport at 26°N over the 2015-2100 time period (Mecking and  
303 Drijfhout, 2023). The northward ocean heat transport across 26°N decreases by an average of  
304 0.3 PW for the SSP5-8.5 scenario and this represents a 30% decline from the historical value  
305 of 1.0 PW.

306

307 The decline in the thermohaline circulation at 26°N implies that the overturning circulation  
308 south of 26°N, that is in the global circulation outside the North Atlantic, has also changed.

309 The extra-Atlantic circulation converts deep water into upper and intermediate waters so that  
310 the southward deep water flow across 26°N and out of the North Atlantic must ultimately be  
311 converted within the global ocean into upper and intermediate waters that flow back into the  
312 North Atlantic and northward across 26°N. The decline in the North Atlantic thermohaline  
313 circulation at 26°N suggests that this global-scale overturning circulation must also have  
314 changed. Baker et al (2023) have explored how 2 mechanisms converting deep water into  
315 upper water south of 26°N change within CMIP6 simulations. The 2 mechanisms considered  
316 are Southern Ocean upwelling associated with eastward wind stress around Antarctica  
317 (Toggweiler and Samuels, 1993) and Indo-Pacific diffusive upwelling associated with deep  
318 interior mixing (Munk, 1966). Baker et al. found that the wind stress around Antarctica did  
319 not decline enough to account for a reduced 6 Sv upwelling of deep water, in fact there  
320 appeared to be a small increase in Southern Ocean wind stress and upwelling. Instead they  
321 found evidence in the CMIP6 projections that the interior Indo-Pacific upwelling declined  
322 enough to account for reduced conversion of deep waters into thermocline waters. They  
323 attributed such decline to the global warming that increases stratification (Li et al., 2020) and  
324 inhibits vertical mixing and associated upwelling.

325  
326 Overall, the Atlantic and global overturning circulations appear to have declined in CMIP6  
327 projections from 2015 to 2100. The manifestation of these declines at 26°N include a  
328 reduction in the southward transport of NADW and a compensating reduction in the  
329 northward flow of upper and thermocline waters through Florida Straits. The reduction in  
330 southward deep water transport in CMIP6 is linked to a lack of INADW formed in the Nordic  
331 Seas flowing out over the Greenland-Iceland-Scotland Ridge into the northern Atlantic  
332 (Heuzé, 2021); and the reduction in northward flow of upper waters is linked to a decrease in  
333 diffusive upwelling in the Indo-Pacific related to increased stratification due to global  
334 warming (Li et al., 2020; Baker et al., 2023). The ability of coupled climate models to  
335 realistically include these critical processes of deep water formation, mixing in ridge  
336 overflows and mid-ocean diffusive upwelling for future projections of ocean circulation  
337 should be carefully assessed. In particular, the representation of deep water formation  
338 in coupled climate models could be examined in comparison with observed production of  
339 deep water. Implementing mixing parameterisations for overflows (Holt et al., 2017) in  
340 coupled climate models could be assessed for their effectiveness in allowing the southward  
341 transport of INADW into and through the North Atlantic. And coupled climate models could  
342 be examined for their parameterisations of diffusive mixing and upwelling, testing how  
343 different parameterisations affect the global ocean overturning circulation over century time  
344 scales.

345  
346 In terms of observations, our results suggest that the ongoing RAPID project should  
347 separately measure the Antilles Current and add it to Florida Straits transport for a true  
348 measure of western boundary current transport for comparison with modelled transport  
349 components. And the Antilles Current transport should be separated from the net mid-ocean  
350 southward flow across 26N in the upper 800m that RAPID labels thermocline recirculation so  
351 as to identify the actual mid-ocean thermocline recirculation associated with the wind stress  
352 curl. By separately estimating the Antilles Current transport contribution, the RAPID project  
353 could then provide well-defined estimates for the wind-driven and thermohaline contributions  
354 to the AMOC at 26°N.

### 355 356 **Code Availability**

357  
358 The code used to obtain the results of this study and a file containing metadata of the models

359 is freely available on GitHub: [https://github.com/jordibeunk/MSc\\_Thesis.git](https://github.com/jordibeunk/MSc_Thesis.git)

360

## 361 **Data Availability**

362 RAPID data and notes are freely available at

363 [https://rapid.ac.uk/rapidmoc/rapid\\_data/datadl.php](https://rapid.ac.uk/rapidmoc/rapid_data/datadl.php)

364 19 CMIP6 models are used. CMIP6 data was accessed and analysed using the super-data-  
365 cluster JASMIN (Lawrence et al. 2013). The choice of these models is motivated by the fact  
366 that both historical (2004-2015) data and future (2015-2100) projections under Shared  
367 Socioeconomic Pathway 5-8.5 are available for all used variables. The model data has been  
368 accessed through the Centre for Environmental Data Analysis (CEDA) archive  
369 <https://data.ceda.ac.uk>

## 370 **Author Contributions**

371

372 This work is based on an MSc thesis by Jordi Beunk at Utrecht University. Jennifer Mecking,  
373 Sybren Drijfhout and Harry Bryden designed the Masters project. Sybren Drijfhout and  
374 Wilco Hazeleger identified the student and supervised the project in Utrecht while Mecking  
375 and Bryden provided advice during the project and write-up of the thesis. After finishing the  
376 thesis, Jordi Beunk initially indicated that he did not wish to write up the results for  
377 publication. Harry Bryden prepared a draft for this paper based on Beunk's thesis. Drijfhout,  
378 Hazeleger and Mecking then edited the draft and all authors added elements of discussion  
379 related to recent papers based on CMIP6 results. Beunk at a late stage indicated he would like  
380 to participate in publishing this work and all authors contributed to revising the work in  
381 response to Referee comments.

382

## 383 **Competing interests**

384

385 The contact author declares that none of the authors has any competing interests

386

## 387 **Acknowledgments**

388 UK Natural Environment Research Council, US National Science Foundation and US  
389 National Oceanic and Atmospheric Administration provide funding for the RAPID project  
390 and make the data freely available. We acknowledge the World Climate Research Programme,  
391 which, through its Working Group on Coupled Modelling, coordinated and promoted CMIP6. We  
392 thank the climate modelling groups for producing and making available their model output, the Earth  
393 System Grid Federation (ESGF) for archiving the data and providing access, and the multiple funding  
394 agencies who support CMIP6 and ESGF. Bryden was a lead investigator for the NERC-funded  
395 project that first deployed the transocean Rapid instrument array in 2004 under grant  
396 NER/T/S/2002/00481 and he has continued to carry out analyses involving the ongoing Rapid  
397 observations following formal retirement in 2011. Drijfhout and Mecking have been funded  
398 by NERC under the Wider Impacts of Subpolar North Atlantic decadal variability on the  
399 ocean and atmosphere (WISHBONE) grant NE/T0133478/1.

400

## 401 **References**

402

403 Asbjørnsen, H. and Årthun, M.: Deconstructing future AMOC decline at 26.5 N, *Geophys. Res. Lett.*,

404 50, e2023GL.103515, <https://doi.org/10.1029/2013GL.103515>, 2023.

405

406 Baker, J. S., Bell, M. J., Jackson, L. C., Renshaw, R., Vallis, G. K., Watson, A. J. and Wood, R. A.:  
 407 Overturning pathways control AMOC weakening in CMIP6 Models, *Geophys. Res. Lett.*, 50,  
 408 e2023GL.103381, <https://doi.org/10.1029/2023GL.103381>, 2023.

409

410 Beunk, J.: Comparing observed and modeled decomposition of the Atlantic Meridional Overturning  
 411 Circulation at 26°N, MSc Thesis, Department of Geosciences, Utrecht University, 54p, 2022.

412

413 Boucher, O., Denvil, S., Levavasseur, G., Cozic, A., Caubel, A., Foujols, M.-A., Meurdesoif, Y.,  
 414 Balkanski, Y., Checa-Garcia, R., Hauglustaine, D., Bekki, S., and Marchand, M.: IPSL IPSL-CM6A-LR-  
 415 INCA model output prepared for CMIP6 CMIP Historical, Version 20211003, Earth System Grid  
 416 Federation, <https://doi.org/10.22033/ESGF/CMIP6.13601>, 2021.

417

418 Boucher, O., Denvil, S., Levavasseur, G., Cozic, A., Caubel, A., Foujols, M.-A., Meurdesoif, Y., Cadule,  
 419 P., Devilliers, M., Dupont, E., and Lurton, T.: IPSL IPSL-CM6A-LR model output prepared for CMIP6  
 420 Scenario MIP ssp585, Version 20211003, Earth System Grid Federation,  
 421 <https://doi.org/10.22033/ESGF/CMIP6.5271>, 2019.

422

423 Bryden, H. L.: Wind-driven and buoyancy-driven circulation in the subtropical North Atlantic  
 424 Ocean, *Proc. Roy. Soc. A*, 477(2256), 20210172, <https://doi.org/10.1098/rspa.2021.0172>, 2021.

425

426 Buckley, M. W., and Marshall, J.: Observations, inferences, and mechanisms of the Atlantic  
 427 Meridional Overturning Circulation: A review, *Rev. Geophys.*, 54(1), 5-63,  
 428 <https://doi.org/10.1002/2015RG000493>, 2016.

429

430 Cao, J.: NUIST NESMv3 model output prepared for CMIP6 ScenarioMIP ssp585, Version 20211003,  
 431 Earth System Grid Federation. <https://doi.org/10.22033/ESGF/CMIP6.8790>, 2019.

432

433 Cao, J, and Wang, B.: NUIST NESMv3 model output prepared for CMIP6 CMIP historical, Version  
 434 20211003, Earth System Grid Federation, <https://doi.org/10.22033/ESGF/CMIP6.8769>, 2019.

435

436 Chai, Z.: CAS CAS-ESM1.0 model output prepared for CMIP6 CMIP historical, Version 20211003,Earth  
 437 System Grid Federation, <https://doi.org/10.22033/ESGF/CMIP6.3353>, 2020.

438

439 Unknown: CAS CAS-ESM1.0 model output prepared for CMIP6 ScenarioMIP ssp585, Earth  
 440 System Grid Federation, [http://cera-www.dkrz.de/WDCC/meta/CMIP6/CMIP6.ScenarioMIP.CAS.CAS-  
 441 ESM2-0.ssp585](http://cera-www.dkrz.de/WDCC/meta/CMIP6/CMIP6.ScenarioMIP.CAS.CAS-ESM2-0.ssp585), 2018.

442

443 Danabasoglu, G.: NCAR CESM2-WACCM model output prepared for CMIP6 ScenarioMIP  
 444 ssp585, Version 20211003, Earth System Grid Federation,  
 445 <https://doi.org/10.22033/ESGF/CMIP6.10115>, 2019.

446

447 Danabasoglu, G.: NCAR CESM2-WACCM-FV2 model output prepared for CMIP6 CMIP  
 448 Historical, Version 20211003, Earth System Grid Federation.  
 449 <https://doi.org/10.22033/ESGF/CMIP6.11298>, 2019.

450

451 DiNezio, P. N., Gramer, L. J., Johns, W. E., Meinen, C. S., and Baringer, M. O.: Observed  
 452 interannual variability of the Florida Current: Wind forcing and the North Atlantic Oscillation. *J.*  
 453 *Phys. Oceanogr.*, 39(3), 721-736, 2009.

454

455 Ditlevsen, P., and Ditlevsen, S.: Warning of a forthcoming collapse of the Atlantic meridional

456 overturning circulation, *Nature Comm.*, 14:4254, <https://doi.org/10.1038/s41467-023-39810-w>,  
457 2023.  
458  
459 EC-Earth Consortium (EC-Earth): EC-Earth-Consortium EC-Earth3 model output prepared for  
460 CMIP6 ScenarioMIP ssp585, Version 20211003, Earth System Grid Federation.  
461 <https://doi.org/10.22033/ESGF/CMIP6.4912>, 2019.  
462  
463 EC-Earth Consortium (EC-Earth): EC-Earth-Consortium EC-Earth-3-CC model output prepared  
464 for CMIP6 CMIP historical, Version 20211003, Earth System Grid Federation,  
465 <https://doi.org/10.22033/ESGF/CMIP6.4702>, 2021.

466 Eyring, V., Bony, S., Meehl, G. A., Senior, C. A., Stevens, B., Stouffer, R. J., and Taylor, K. E.: Overview  
467 of the Coupled Model Intercomparison Project Phase 6 (CMIP6) experimental design and  
468 organization, *Geoscientific Model Development*, 9(LLNL-JRNL-736881), 1937–1958,  
469 <https://doi.org/10.5194/gmd-9-1937-2016>, 2016.

470 Good, P.: MOHC HadGEM3-GC31-LL model output prepared for CMIP6 ScenarioMIP  
471 ssp585. Version 20211003. Earth System Grid Federation.  
472 <https://doi.org/10.22033/ESGF/CMIP6.10901>, 2020.  
473  
474 Good, P., Sellar, A., Tang, Y., Rumbold, S., Ellis, R., Kelley, D., and Kuhlbrodt, T.: MOHC UKESM1.0-LL  
475 model output prepared for CMIP6 ScenarioMIP ssp585, Version 20211003, Earth System Grid  
476 Federation, <https://doi.org/10.22033/ESGF/CMIP6.6405>, 2019.

477 Heuzé, C.: Antarctic bottom water and North Atlantic deep water in CMIP6 models. *Ocean Science*,  
478 17(1), 59–90, <https://doi.org/10.5194/os-17-59-2021>, 2021.

479 Holt, J., Hyder, P., Ashworth, M., Harle, J., Hewitt, H. T., Liu, H., New, A. L., Pickles, S., Porter, A.,  
480 Popova, E., Allen, J. I., Siddorn, J., and Wood, R.: Prospects for improving the representation of  
481 coastal and shelf seas in global ocean models, *Geosci. Model Dev.*, 10, 499–523, 2017.

482 Huang, W.: THU CIESM model output prepared for CMIP6 CMIP historical, Version 20211003, Earth  
483 System Grid Federation, <https://doi.org/10.22033/ESGF/CMIP6.8843>, 2019.  
484  
485 Huang, W.: THU CIESM model output prepared for CMIP6 ScenarioMIP ssp585,  
486 Version 20211003, Earth System Grid Federation, <https://doi.org/10.22033/ESGF/CMIP6.8863>, 2020.  
487  
488 Johns, W. E., Baringer, M. O., Beal, L. M., Cunningham, S. A., Kanzow, T., Bryden, H. L., Hirschi, J.  
489 Marotzke, J., Meinen, C., Shaw, B., and Curry, R.: Continuous, array-based estimates of Atlantic  
490 Ocean heat transport at 26.5°N, *J. Clim.*, 24, 2429–2449, doi:10.1175/2010JCLI3997.1, 2011.  
491  
492 Johns, W.E., Elipot, S., Smeed, D. A., Moat, B., King, B., Volkov, D. L., and Smith, R. H.: Towards two  
493 decades of Atlantic Ocean mass and heat transports at 26.5 N, *Phil. Trans. R. Soc. A*, 381,  
494 <https://doi.org/10.1098/rsta.2022.0188>, 2023.  
495  
496 Jungclaus, J., Bittner, M., Wieners, K.-H., Wachsmann, F., Schupfner, M., Legutke, S., Giorgetta, M.;  
497 Reick, C., Gayler, V., Haak, H., de Vrese, P., Raddatz, T., Esch, M., Mauritsen, T., von Storch, J.-S.,  
498 Behrens, J., Brovkin, V., Claussen, M., Crueger, T., Fast, I., Fiedler, S., Hagemann, S., Hohenegger, C.,  
499 Jahns, T., Kloster, S., Kinne, S., Lasslop, G., Kornblueh, L., Marotzke, J., Matei, D., Meraner, K.,  
500 Mikolajewicz, U., Modali, K., Müller, W., Nabel, J., Notz, D., Peters-von Gehlen, K., Pincus, R.,  
501 Pohlmann, H., Pongratz, J., Rast, S., Schmidt, H., Schnur, R., Schulzweida, U., Six, K., Stevens, B., Voigt,

502 A., and Roeckner, E.: MPI-M MPI-ESM1.2-HR model output prepared for CMIP6 CMIP historical,  
503 Version 20211003, Earth System Grid Federation, <https://doi.org/10.22033/ESGF/CMIP6.6594>, 2019.

504

505 Lawrence, B. N.: Storing and manipulating environmental big data with JASMIN. in *2013 IEEE*  
506 *International Conference on Big Data* 68–75 (ieeexplore.ieee.org, 2013),  
507 doi:10.1109/BigData.2013.6691556.

508

509 Lee, J.-Y., J. Marotzke, J., Bala, G., Cao, L., Corti, S., Dunne, J.P., Engelbrecht, F., Fischer, E., Fyfe, J.C.,  
510 Jones, C., Maycock, A., Mutemi, J., Ndiaye, O., Panickal, S., and Zhou, T.: Future Global Climate:  
511 Scenario-Based Projections and Near- Term Information. In *Climate Change 2021: The Physical*  
512 *Science Basis. Contribution of Working Group I to the Sixth Assessment Report of the*  
513 *Intergovernmental Panel on Climate Change* [Masson-Delmotte, V., Zhai, P., Pirani, A., Connors, S.L.,  
514 Péan, C., Berger, S., Caud, N., Chen, Y., Goldfarb, L., Gomis, M. I., Huang, M., Leitzell, K., Lonnoy, E.,  
515 Matthews, J. B. R., Maycock, T. K.; Waterfield, T., Yelekçi, O., Yu, R., and Zhou, B. (eds.)]. Cambridge  
516 University Press, Cambridge, United Kingdom and New York, NY, USA, pp. 553–672,  
517 doi:10.1017/9781009157896.006, 2021

518

519 Levang, S. J., and Schmitt, R. W.: What Causes the AMOC to Weaken in CMIP5? *J. Clim.*, *33*(4), 1535-  
520 1545, 2020.

521

522 Li, G., Cheng, L., Zhu, J., Trenberth, K. E., Mann, M. E. and Abraham, J. P.: Increasing ocean  
523 stratification over the past half-century, *Nat. Clim. Change* *10*, 1116–1123, 2020.

524

525 Lovato, T., and Peano, D.: CMCC CMCC-CM2-SR5 model output prepared for CMIP6, CMIP historical,  
526 Version 20211003, Earth System Grid Federation, <https://doi.org/10.22033/ESGF/CMIP6.3825>, 2020.

527

528 Lovato, T., and Peano, D.: CMCC CMCC-CM2-SR5 model output prepared for CMIP6, ScenarioMIP  
529 ssp585, Version 20211003, Earth System Grid Federation,  
530 <https://doi.org/10.22033/ESGF/CMIP6.3896>, 2020.

531

532 Lovato, T., Peano, D., and Butenschön, M.: CMCC CMCC-ESM2 model output prepared for CMIP6  
533 CMIP historical, Version 20211003, Earth System Grid Federation.  
534 <https://doi.org/10.22033/ESGF/CMIP6.13195>, 2021.

535

536 Lovato, T., Peano, D., and Butenschön, M.: CMCC CMCC-ESM2 model output prepared for CMIP6  
537 ScenarioMIP ssp585, Version 20211003, Earth System Grid Federation.  
538 <https://doi.org/10.22033/ESGF/CMIP6.13259>, 2021.

539

540 McCarthy, G. D., and Caesar, L.: Can we trust projections of AMOC weakening based on climate  
541 models that cannot reproduce the past?, *Phil. Trans. Roy. Soc.*, 381(2262),  
542 <https://doi.org/10.1098/rsta.2022.0193>, 2023.

543

544 McCarthy, G. D., Smeed, D. A., Johns, W. E., Frajka-Williams, E., Moat, B. I., Rayner, D., Baringer, M.  
545 O., Meinen, C. S., and Bryden, H. L.: Measuring the Atlantic meridional overturning circulation at  
546 26°N, *Prog. Oceanogr.*, *130*, 91-111, doi:10.1016/j.pocean.2014.10.006, 2015..

547

548 Mecking, J.V. and Drijfhout, S. S.: The decrease in ocean heat transport in response to global  
549 warming, *Nat. Clim. Change*, *13*. 1229-1236, <https://doi.org/10.1038/s41558-023-01829-8>, 2023.

550

551 Meinen, C. S., Johns, W. E., Moat, B. I., Smith, R. H., Johns, E. M., Rayner, D., Frajka-Williams, E.,  
552 Garcia, R. F., and Garzoli, S. L.: Structure and variability of the Antilles Current at 26.5 N, *J. Geophys.*  
553 *Res. Oceans*, *124*, 3700-3723, doi:10.1029/2018JC014836, 2019.

554  
555 Moat B. I., Smeed, D. A., Frajka-Williams, E., Desbruyeres, D. G., Beaulieu, C., Johns, W. E., Rayner, D.,  
556 Sanchez-Franks, A., Baringer, M. O., Volkov, D., Jackson, L. C., and Bryden, H.L.: Pending recovery in  
557 the strength of the meridional overturning circulation at 26°N. *Ocean Sci.* 16, 863–874,  
558 [doi:10.5194/os-16-863-2020](https://doi.org/10.5194/os-16-863-2020), 2020.

559  
560 Moat, B. I., Frajka-Williams, E., Smeed, D. A., Rayner, D., Johns, W. E., Baringer, M. O., Volkov, D. L.,  
561 and Collins, J.: Atlantic meridional overturning circulation observed by the RAPID-MOCHA-WBTS  
562 (RAPID-meridional Overturning Circulation and Heatflux Array-Western Boundary Time Series) array  
563 at 26N from 2004 to 2020 (v2020.2). British Oceanographic Data Centre, Natural Environment  
564 Research Council [data set]. <https://doi.org/10.5285/e91b10af-6f0a-7fa7-e053-6c86abc05a09>, 2022.

565  
566 Munk, W.: Abyssal recipes. *Deep-Sea Res.*, 13, 707-730, 1966.

567  
568 O'Neill, B. C., Tebaldi, C., Vuuren, D. P. V., Eyring, V., Friedlingstein, P., Hurtt, G., Knutti, R., Kriegler,  
569 E., Lamarque, J.-F., Lowe, J., Meehl, G. A., Moss, R., Riahi, K., and Sanderson, B. M.: The scenario  
570 model intercomparison project (ScenarioMIP) for CMIP6, *Geoscientific Model Development*, 9(9),  
571 3461–3482 <https://doi.org/10.5194/gmd-9-3461-2016>, 2016.

572  
573 Piecuch, C. G., and Beal, L. M.: Robust Weakening of the Gulf Stream During the Past Four Decades  
574 Observed in the Florida Straits, *Geophys. Res. Lett.*, 50, <https://doi.org/10.1029/2023gl105170>, 2023.

575  
576 Ridley, J., Menary, M., Kuhlbrodt, T., Andrews, M., and Andrews, T.: MOHCHadGEM3-GC31-LL model  
577 output prepared for CMIP6 CMIP historical, Version 20211003, Earth System Grid Federation,  
578 <https://doi.org/10.22033/ESGF/CMIP6.6109>, 2019.

579  
580 Ridley, J., Menary, M., Kuhlbrodt, T., Andrews, M., Andrews, T.: MOHCHadGEM3-GC31-MM model  
581 output prepared for CMIP6 CMIP historical, Version 20211003, Earth System Grid Federation,  
582 <https://doi.org/10.22033/ESGF/CMIP6.6112>, 2019.

583  
584 Roberts, M. J., Jackson, L. C., Roberts, C. D., Meccia, V., Docquier, D., Koenigk, T., Ortega, P., Moreno-  
585 Chamarro, E., Bellucci, A., Coward, A., Drijfhout, S., Exarchou, E., Gutjahr, O., Hewitt, H., Iovino, D.,  
586 Lohmann, K., Putrasahan, D., Schiemann, R., Seddon, J., Terray, L., Xu, X., Zhang, Q., Chang, P.,  
587 Yeager, S. G., Castruccio, F. S., Zhang, S., and Wu, L.: Sensitivity of the Atlantic meridional  
588 overturning circulation to model resolution in CMIP6 HighResMIP simulations and implications for  
589 future changes, *J. Adv. Modeling Earth Sys.*, 12(8), e2019MS002014, 2020.

590  
591 Rong, X.: CAMS CAMS\_CSM1.0 model output prepared for CMIP6 CMIP historical, Version 20211003,  
592 Earth System Grid Federation. <https://doi.org/10.22033/ESGF/CMIP6.9754>, 2019.

593  
594 Rong, X.: CAMS CAMS-CSM1.0 model output prepared for CMIP6 ScenarioMIP ssp585,  
595 Version 20211003, Earth System Grid Federation, <https://doi.org/10.22033/ESGF/CMIP6.11052>,  
596 2019.

597  
598 Schupfner, M., Wieners, K.-H., Wachsmann, F., Steger, C., Bittner, M., Jungclaus, J., Früh, B., Pankatz,  
599 K., Giorgetta, M., Reick, C., Legutke, S., Esch, M., Gayler, V., Haak, H., de Vrese, P., Raddatz, T.,  
600 Mauritsen, T., von Storch, J.-S., Behrens, J., Brovkin, V., Claussen, M., Crueger, T., Faust, I., Fiedler, S.,  
601 Hagemann, S., Hohenegger, C., Jahns, T., Kloster, S., Kinne, S., Lasslop, G., Kornbluh, L., Marotzke, J.,  
602 Matei, D., Meraner, K., Mikolajewicz, U., Modali, K., Müller, W., Nabel, J., Notz, D., Peters-von  
603 Gehlen, K., Pincus, R., Pohlmann, H., Pongratz, J., Rast, S., Schmidt, H., Schnur, R., Schulzweida, U.,

604 Six, K., Stevens, B., Voigt, A., and Roeckner, E.: DKRZ MPI-ESM1.2-HR model output prepared for  
605 CMIP6 ScenarioMIPssp585, Version 20211003, Earth System Grid Federation.  
606 <https://doi.org/10.22033/ESGF/CMIP6.4403>, 2019.  
607

608 Seferian, R.: CNRM-CERFACS CNRM-ESM2-1 model output prepared for CMIP6 CMIP Historical,  
609 Version 20211003, Earth System Grid Federation. <https://doi.org/10.22033/ESGF/CMIP6.4068>, 2018.  
610

611 Smeed, D. A., Josey, S. A., Beaulieu, C., Johns, W.E., Moat, B. I., Frajka-Williams, E., Rayner, D.,  
612 Meinen, C. S., Baringer, M. O., Bryden, H. L., and McCarthy, G. D.: The North Atlantic Ocean is in a  
613 state of reduced overturning, *Geophys. Res. Lett.*, 45, <https://doi.org/10.1002/2017GL076350>, 2018.  
614

615 Song, Z., Qiao, F., Bao, Y., Shu, Q., Song, Y., and Yang, X.: FIO-QLNM FIO-ESM2.0 model output  
616 prepared for CMIP6 CMIP historical. Version 20211003. Earth System Grid  
617 Federation. <https://doi.org/10.22033/ESGF/CMIP6.9199>, 2019.  
618

619 Song, Z., Qiao, F., Bao, Y., Shu, Q., Song, Y., and Yang, X.: FIO-QLNM FIO-ESM2.0 model output  
620 prepared for CMIP6 ScenarioMIP ssp585, Version 20211003, Earth System Grid  
621 Federation. <https://doi.org/10.22033/ESGF/CMIP6.9214>, 2019.  
622

623 Stommel, H.: The westward intensification of wind-driven ocean currents. *Eos, Trans. American*  
624 *Geophys. Union*, 29(2), 202-206, 1948.  
625

626 Swart, N. C., Cole, J. N. S., Kharin, V. V., Lazare, M., Scinocca, J. F., Gillett, N. P., Anstey, J., Arora, V.,  
627 Christian, J. R., Jiao, Y., Lee, W. G., Majaess, F., Saenko, O. A., Seiler, C., Seinen, C., Shao, A., Solheim,  
628 L., von Salzen, K., Yang, D., Winter, B., and Sigmund, M.: CCCma CanESM5 model output prepared for  
629 CMIP6 CMIP historical, Version 20211003, Earth System Grid Federation,  
630 <https://doi.org/10.22033/ESGF/CMIP6.3610>, 2019.  
631

632 Swart, N. C., Cole, J. N. S., Kharin, V. V., Lazare, M., Scinocca, J. F., Gillett, N. P., Anstey, J., Arora, V.,  
633 Christian, J. R., Jiao, Y., Lee, W. G., Majaess, F., Saenko, O. A., Seiler, C., Seinen, C., Shao, A., Solheim,  
634 L., von Salzen, K., Yang, D., Winter, B., and Sigmund, M.: CCCma CanESM5 model output prepared for  
635 CMIP6 ScenarioMIP ssp585, Version 20211003, Earth System Grid Federation.  
636 <https://doi.org/10.22033/ESGF/CMIP6.3696>, 2019.  
637

638 Tang, Y., Rumbold, S., Ellis, R., Kelley, D., Mulcahy, J., Sellar, A., Walton, J., and Jones, C.: MOHC  
639 UKESM1.0-LL model output prepared for CMIP6 CMIP Historical, Version 20211003 Earth System  
640 Grid Federation, <https://doi.org/10.22033/ESGF/CMIP6.6113>, 2019.

641 Toggweiler, J. R., and Samuels, B.: On the ocean's large-scale circulation near the limit of no vertical  
642 mixing, *J. Phys. Oceanogr*, 28(9), 1832–1852. [https://doi.org/10.1175/1520-0485\(1998\)028](https://doi.org/10.1175/1520-0485(1998)028), 1998.

643 Voldoire, A.: CNRM-CERFACS CNRM-CM6-1-HR model output prepared for CMIP6 CMIP  
644 Historical, Version 20211003, Earth System Grid Federation,  
645 <https://doi.org/10.22033/ESGF/CMIP6.4067>, 2019.  
646

647 Voldoire, A.: CNRM-CERFACS CNRM-CM6-1-HR model output prepared for CMIP6 ScenarioMIP  
648 ssp585, Version 20211003, Earth System Grid Federation.  
649 <https://doi.org/10.22033/ESGF/CMIP6.4225>, 2019.  
650

651 Weijer, W., Cheng, W., Garuba, O. A., Hu, A., and Nadiga, B. T.: CMIP6 models predict significant  
652 21st century decline of the Atlantic Meridional Overturning Circulation, *Geophys. Res.*  
653 *Lett.*, 47(12), doi:10.1002/2019GL086075, 2020.

654  
655 Wieners, K.-H., Giorgetta, M., Jungclaus, J., Reick, C., Esch, M., Bittner, M., Legutke, S., Schupfner, M.,  
656 Wachsmann, F., Gayler, V., Haak, H., de Vrese, P., Raddatz, T., Mauritsen, T., von Storch, J.-S.,  
657 Behrens, J., Brovkin, V., Claussen, M., Crueger, T., Fast, I., Fiedler, S., Hagemann, S., Hohenegger, C.,  
658 Jahns, T., Kloster, S., Kinne, S., Lasslop, G., Kornblueh, L., Marotzke, J., Matei, D., Meraner, K.,  
659 Mikolajewicz, U., Modali, K., Müller, W., Nabel, J., Notz, D., Peters-von Gehlen, K., Pincus, R.,  
660 Pohlmann, H., Pongratz, J., Rast, S., Schmidt, H.; Schnur, R., Schulzweida, U., Six, K., Stevens, B., Voigt,  
661 A., and Roeckner, E.: MPI-M MPI-ESM1.2-LR model output prepared for CMIP6 CMIP historical,  
662 Version 20211003, Earth System Grid Federation, <https://doi.org/10.22033/ESGF/CMIP6.6595>, 2019.  
663  
664 Wieners, K.-H., Giorgetta, M., Jungclaus, J., Reick, C., Esch, M., Bittner, M., Gayler, V., Haak, H., de  
665 Vrese, P., Raddatz, T., Mauritsen, T., von Storch, J.-S., Behrens, J., Brovkin, V., Claussen, M., Crueger,  
666 T., Fast, I., Fiedler, S., Hagemann, S., Hohenegger, C., Jahns, T., Kloster, S., Kinne, S., Lasslop, G.,  
667 Kornblueh, L., Marotzke, J., Matei, D., Meraner, K., Mikolajewicz, U., Modali, K., Müller, W., Nabel, J.,  
668 Notz, D., Peters-von Gehlen, K., Pincus, R., Pohlmann, H., Pongratz, J., Rast, S., Schmidt, H., Schnur,  
669 R., Schulzweida, U., Six, K., Stevens, B., Voigt, A., and Roeckner, E.: MPI-M MPI-ESM1.2-LR model  
670 output prepared for CMIP6 ScenarioMIP ssp585, Version 20211003, Earth System Grid Federation,  
671 <https://doi.org/10.22033/ESGF/CMIP6.6705>, 2019.  
672  
673 Yan, X., Zhang, R., and Knutson, T. R.: Underestimated AMOC variability and implications for  
674 AMV and predictability in CMIP models, *Geophys. Res. Lett.*, *45*(9), 4319-4328, 2018.  
675  
676 Yukimoto, S., Koshiro, T., Kawai, H., Oshima, N., Yoshida, K., Urakawa, S., Tsujino, H., Deushi, M.,  
677 Tanaka, T., Hosaka, M., Yoshimura, H., Shindo, E., Mizuta, R., Ishii, M., Obata, A., and Adachi, Y.: MRI  
678 MRI-ESM2.0 model output prepared for CMIP6 CMIP historical, Version 20211003, Earth System Grid  
679 Federation, <https://doi.org/10.22033/ESGF/CMIP6.6842>, 2019.  
680  
681 Yukimoto, S., Koshiro, T., Kawai, H., Oshima, N., Yoshida, K., Urakawa, S., Tsujino, H., Deushi, M.,  
682 Tanaka, T., Hosaka, M., Yoshimura, H., Shindo, E., Mizuta, R., Ishii, M., Obata, A., and Adachi, Y.: MRI  
683 MRI-ESM2.0 model output prepared for CMIP6 ScenarioMIP ssp585, Version 20211003, Earth System  
684 Grid Federation, <https://doi.org/10.22033/ESGF/CMIP6.6929>, 2019.  
685  
686 Zhao, J., and Johns, W.: Wind-forced interannual variability of the Atlantic Meridional Overturning  
687 Circulation at 26.5 N, *J. Geophys. Res. Oceans*, *119*, 2403-2419, doi:10.1002/2013JC009407, 2014.  
688  
689  
690